Hindawi
Journal of Nanomaterials
Volume 2023, Article ID 8200912, 9 pages
https://doi.org/10.1155/2023/8200912

Research Article

Garlic Extract-Mediated Synthesis of ZnS Nanoparticles: Structural, Optical, Antibacterial, and Hemolysis Studies

Adnan Alnehia,[1,2] **Abdel-Basit Al-Odayni**,[3,4] **A. H. Al-Hammadi**,[1] **Safiah A. Alramadhan**,[3,5] **Hisham Alnahari**,[1] **Waseem Sharaf Saeed**,[3] **and Annas Al-Sharabi**[2]

[1]*Department of Physics, Faculty of Sciences, Sana'a University, Sana'a 12081, Yemen*
[2]*Department of Physics, Faculty of Applied Sciences, Thamar University, Dhamar 87246, Yemen*
[3]*Engineer Abdullah Bugshan Research Chair for Dental and Oral Rehabilitation, College of Dentistry, King Saud University, Riyadh 11545, Saudi Arabia*
[4]*Department of Chemistry, Faculty of Education, Thamar University, Dhamar 87246, Yemen*
[5]*Umm Al-Momineen Maimouna Bint Al-Harth Intermediate School at the National Guard, Al Khobar Education Office, General Directorate of Education Eastern Province, Ministry of Education, Al Khobar, Saudi Arabia*

Correspondence should be addressed to Annas Al-Sharabi; annas.alsharabi3@gmail.com

Received 12 October 2022; Revised 13 December 2022; Accepted 14 December 2022; Published 12 February 2023

Academic Editor: Abdelwahab Omri

The green synthesis of zinc sulfide nanoparticles (ZnS NPs)-mediated plant extract is gaining importance because of its simplicity, cost-effectiveness, and ecofriendly nature. In this work, ZnS NPs were synthesized using garlic extract as NPs facilitating agent, characterized by Fourier transform infrared, X-ray diffraction, scanning electron microscope, and UV–visible, then their antibacterial and hemocompatibility were assayed. Analysis revealed a cubic phase, 2.33 nm crystallite size, and a 3.75 eV optical bandgap. Bioactivity test against *Staphylococcus aureus* and *Escherichia coli* indicated dose-dependent potency closer to that of azithromycin standard drug and more efficient on *S. aureus* (Gram-positive) than *E. coli* (Gram-negative) bacteria. Biocompatibility test in terms of erythrocyte hemolysis, in reference to normal saline and water as minimal and maximal controls, confirmed nontoxic substance up to 100 μg/mL as the highest examined concentration and at which a lysis of 2.9% was detected. Therefore, it could be concluded that this biogenic method is effective in producing ZnS NPs with desirable properties for potential biomedical applications.

1. Introduction

Green chemistry for sustainable development has gained greater interest in the last few years with researchers aim to reduce hazards via developing of greener methods for nanomaterials biosynthesis using plants as one simple and ecofriendly approach [1]. In principle, the synthesis of nanomaterials demands a selection of (1) adequate solvent, (2) a good reducing agent, and (3) a good stabilizing agent. Although various chemical methods can be applied for the synthesis of NPs, bio-approach is considered safer, ecofriendly, and low cost. Therefore, plant-mediated synthesis of NPs has become an innovative industrial technique with plenty of benefits due to plant obtainability and uncostly, the method simplicity and scaling up possibility, and the NPs obtained size and shape tailorability [2, 3].

Plant-based biosynthesis of NPs basically involves the application of plant extracts to reduce and stabilize metal ions through some implicated plant phytocompounds like amino acids, alkaloids, enzymes, saponins, terpenoids, phenolics [4, 5], etc. ZnS is a promising semiconductor with a wide bandgap, which benefiting electronic, optoelectronic, and electrochemical devices [6]. ZnS NPs commonly show distinct features different from its bulk counterpart as a result of high surface-to-volume ratio [7]. It can be synthesized by various methods such as physical, chemical, and biological approaches [8–10]. While physical routes such as thermal evaporation [11], pulsed laser vaporization [12],

and molecular beam epitaxy [13] and chemical methods like coprecipitation [14], sol–gel [9], sonochemical [15], and hydrothermal [10] are widely employed, biosynthesis is still in its advent. In addition, the conventional physical and chemical methods are expensive and release hazardous materials into the environment [16]; hence, to reduce such risk, biosynthesis has been considered the most reliable and safe method. Furthermore, green synthesis has become preferred as it is quick and suitable for large-scale production, with plant-based extract being most applicable for NPs size and shape control as driven by their phytochemical compounds [17–19]. Bioactivity studies on ZnS NPs have reported significant action against number of test bacteria, being more effective on Gram-positive bacteria, and nontoxic against human erythrocytes [20].

Many studies have illustrated the feasibility of using plant extracts (seed, leaves, and roots) as a capping agent in the synthesis of nanomaterials with certain properties and applications [21–23]. In this regard, ZnS NPs have been the subject of many plant-based biosynthesis studies, of which garlic extract-based was a promising route [20, 24, 25]. Garlic, *Allium sativum*, is a spice widely used as a food and as a medicinal agent. It is one of the most extensively researched vegetables. It has acquired a reputation as a formidable prophylactic and therapeutic medicinal agent in the folklore of many cultures. It is rich in several sulfur-containing phytoconstituents such as alliin, allicin, ajoenes, vinyldithiins, and flavonoids such as quercetin [26, 27], with aqueous extract having abundance of *S*-allyl mercapto cysteine and glucose, those may play an important role on NPs production via contribution on capping and stabilizing process [28]. Accordingly, garlic extract can be used as NPs synthesis facilitating agent, where allicin and other carbohydrates are the primary stabilizing moieties [29].

To the best of our knowledge, phytosynthesis of ZnS NPs using garlic-based aqueous extract, and their bioactivity studies, are not well documented. Therefore, the main objective of this work is to utilize garlic aqueous extract for the synthesis of ZnS NPs and to investigate their physicochemical and biological properties. The biogenic ZnS NPs were characterized for their structural properties using Fourier transform infrared (FTIR), X-ray diffraction (XRD), scanning electron microscope (SEM), and UV–visible (UV–vis) and for their bioactivity using antibacterial and hemolysis assays.

2. Materials and Methods

2.1. Materials. Zinc nitrate hexahydrate ($Zn(NO_3)_2{\cdot}6H_2O$; ≥99%) and sodium sulfide hydrate flakes ($Na_2S{\cdot}xH_2O$; 60%) were purchased from Himedia Laboratories GmbH (Einhausen, Germany). Mueller–Hinton Agar (MHA) was acquired from Sigma–Aldrich (Darmstadt, Germany). Garlic (*A. sativum*) bulbs were collected from a local market that usually sold after a few months of harvesting. Bacteria strains (*Staphylococcus aureus* and *Escherichia coli*) were kindly obtained as a gift from Al-Jarfi Medical Lab (Tamar City, Yemen). Normal saline (NS; 0.9 w/v% sodium chloride; pH 4.5–7.0) was collected from Pharmaceutical Solutions Industry (Jeddah, Saudi Arabia). Deionized water (dH_2O) was used wherever required.

2.2. Preparation of Garlic Extract. Garlic mature bulbs were obtained by local sellers at Thamar city, Yemen, in winter first 2022, cleaned and peeled before grinding. Extraction was carried out following a previously described protocol [7, 30] with some modifications. The peeled bulbs were ground using a houseware electric grinder into fine fragments. Next, 5 g of the obtained *garlic* matter was added into 100 mL dH_2O and mixed with constant stirring at 25°C for 60 min, then filtered to obtain the intended *garlic* extract.

2.3. Green Synthesis of ZnS NPs. The biosynthesis of ZnS NPs was carried out as described in literature [2, 7], with slight modification. Thus, stochiometric (0.02 mol) solutions of zinc nitrate (6 g in 25 mL) and sodium sulfide (2.6 g in 25 mL) were separately prepared by dissolving the corresponding salt in dH_2O with magnetic stirring for 15 min. The two solutions were then mixed together and to which 30 mL of the freshly prepared *garlic* extract was added, then allowed to stir at 25°C for 60 min. The obtained precipitate was then filtered, washed with dH_2O, and dried at 25°C for 48 hr. Finally, the obtained powder was further annealed at 100°C for 60 min. Figure 1 summarizes the overall workflow of the present study, including extract preparation, ZnS NPs synthesis, characterization techniques, and applications.

2.4. Characterization. The XRD pattern was recorded using an XD–2 X-ray diffractometer (Beijing Purkinje General Instrument Co., Ltd., Beijing, China) with CuKα radiation of $\lambda = 1.5418$ Å, over two-theta (2θ) 15°–75° and scanning rate of 0.02 min^{-1}. FTIR spectra were obtained by Nicolet iS10 FTIR spectrometer (Thermo Scientific, Madison, WI, USA) using an attenuated total reflection (ATR) accessory (diamond type) on the range of 650–4,000 cm^{-1}, reported as the average of 32 scans and a resolution of 4 cm^{-1}. Surface morphology was imaged using a JSM-7600F field-emission scanning electron microscope (FESEM) (Jeol Ltd., Tokyo, Japan), where the sample was sputter coated with gold before shoot. UV–vis spectrophotometer (U3900, Hitachi, Tokyo, Japan), coupled with Varian Cary-50 software, was employed for acquiring electronic spectra in the range of 200–800 nm at room temperature.

2.5. Biological Studies

2.5.1. Antibacterial Test. The antibacterial activity of ZnS NPs was carried out via the disc diffusion method [31, 32], against *S. aureus* and *E. coli* bacteria representing Gram-positive and Gram-negative bacteria types, respectively. Thus, the bacterial strains were individually cultured at 37 ± 1°C for 24 hr. The turbidity of the final nutrient broth was adjusted to achieve an absorbance of 0.075–0.1. In this route, 20 mL of sterilized MHA was poured into sterile petri plates; after solidification, the test bacteria were then spread over MHA plate. The test disks of 0.6 cm diameter were wetted by 20 μL on each side of the target ZnS NPs aqueous suspension (63 and

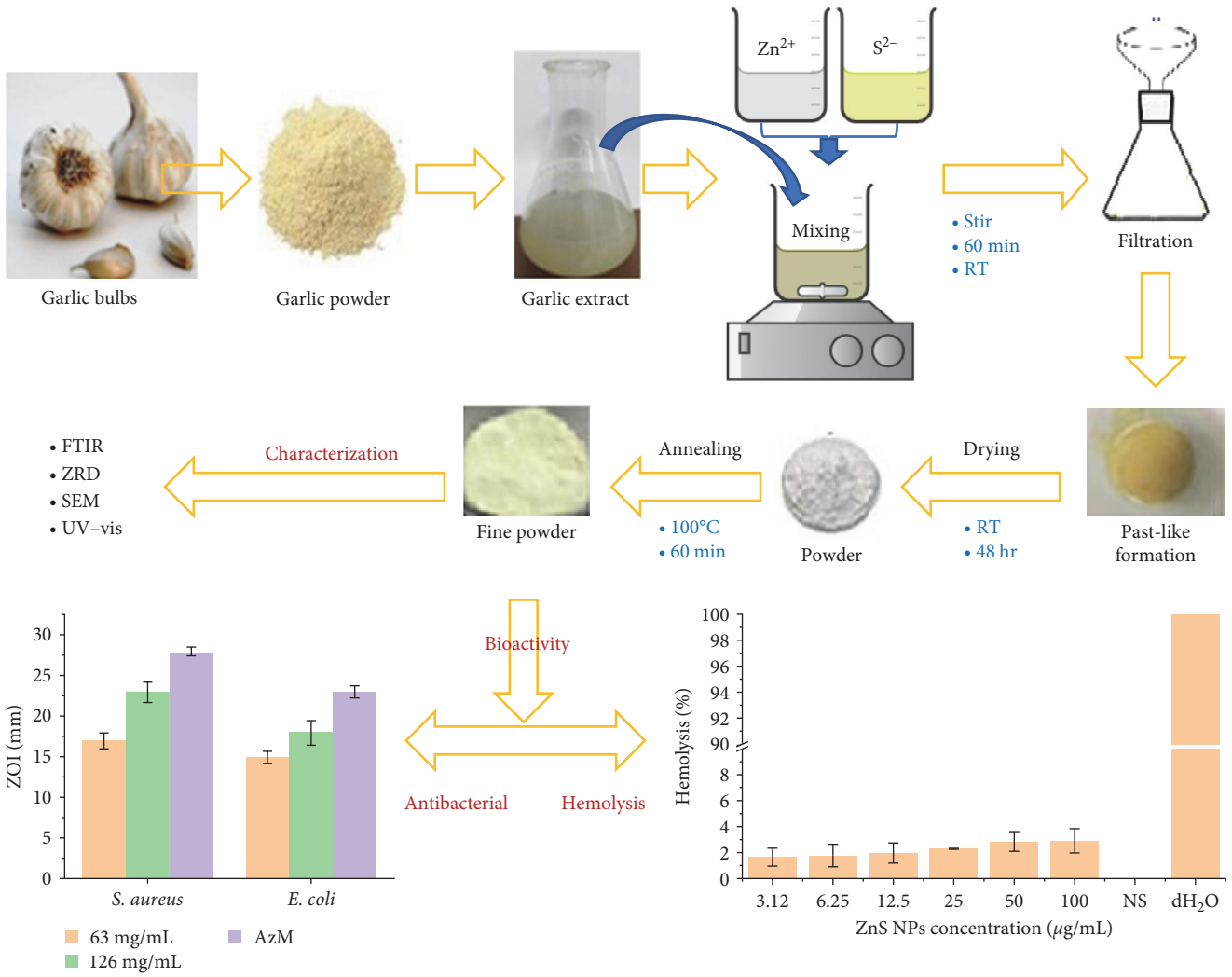

FIGURE 1: Flowchart for the biosynthesis route of ZnS NPs using garlic extract, characterization methods, and the applied bioactivity assays.

126 mg/mL). Then, the disks were dried and placed aseptically on the surface of bacterially seeded petri dishes, which were subsequently incubated at $37 \pm 1°C$ for 21 hr. Azithromycin (AzM) and dH_2O were used as positive and negative control, respectively, and treated similarly and simultaneously with test samples. The inhibitory effect was assessed in terms of zone of inhibition (ZOI) by measuring the inhibition area in mm and compared with the controls as described in literature [33].

2.5.2. Hemolytic Assay. Hemolytic activity of the synthesized ZnS NPs was evaluated against human erythrocytes over a concentration range of 3.12–100 μg/mL. The assay was carried out as previously described [2, 34] with few modifications. Briefly, 5 mL of blood was taken from a healthy male volunteer (25 years old, B-positive blood group) after the provision of informed consent. The collected blood sample was transferred into ethylenediaminetetraacetic acid (EDTA) tube. Then, red blood cells (RBCs) were isolated using a typical procedure described elsewhere. Thus, EDTA-blood suspension was centrifuged for 10 min at 4,000 rpm, decanting the supernatant, and pellet was adequately washed with 0.9% NS solution.

The test erythrocytes suspension was diluted as 2% cells while test samples of ZnS NPs were prepared as 3.12–100 μg/mL in NS. Experimentally, 0.5 mL of the cell suspension was mixed with 0.5 mL of each test sample and immediately incubated at 37°C for 60 min. Afterward, solutions were centrifuged at 4,000 rpm for 10 min to remove cell depression, and the supernatant containing free hemoglobin was photometrically measured at 540 nm. Sterile NS and dH_2O were used as minimal and maximal hemolytic controls, respectively, and were experimentally treated as test samples. The hemolytic percentage was calculated based on Equation (1).

$$\%\text{Hemolysis} = \left(\frac{A_S - A_N}{A_P - A_N}\right) \times 100, \quad (1)$$

where A_S, A_N, and A_P are the absorbance of the ZnS NPs, NS, and dH_2O, respectively.

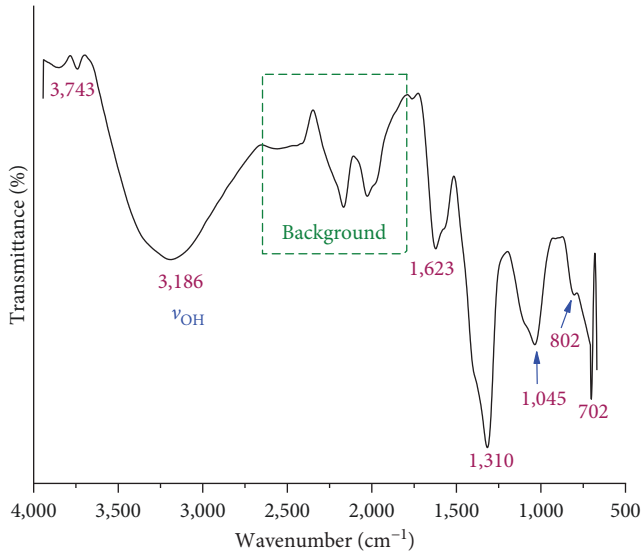

FIGURE 2: FTIR spectra of garlic extract-mediated biosynthesized ZnS NPs.

2.6. Data Analysis. Data for bioactivity (antibacterial ZOI and hemolysis) from two-independent experiments were statistically analyzed using Microsoft Excel, Version 2019 (Microsoft Corporation, WA, USA) and reported as the mean and standard deviation. Presented figures and histograms were drawn in OriginPro 2018 software (Origin Lab, Northampton, MA, USA). ImageJ Version 1.52a (National Institute of Health, Bethesda, MD, USA) was used for counting of particle sizes from FESEM micrograph.

3. Results and Discussion

3.1. FTIR Analysis. Figure 2 illustrates the FTIR spectrum of the biosynthesized ZnS NPs. Due to the capacity limit of the ATR-FTIR instrument, the measuring range was limited to 650–4,000 cm^{-1}. In this range, indicative peaks of the NPs, as well as the traced organics involved in the NPs production, can be identified. The broad band centered at about 3,186 cm^{-1} is characteristic of different hydroxyls (–OH, such as alcohols, phenols, and carboxylic acids) and amines (–NHn) functional groups. Peaks on the wavenumber (e.g., above 3,500 cm^{-1}) are commonly of nonhydrogen bonded OH, while broadness indicates contribution from carboxylic acids [24]. Peaks observed in the range of 1,800–2,600 cm^{-1} are instrument-based backgrounds [35]. The absorption peak at 1,623 cm^{-1} can be attributed to C=C stretching bands associated with alkene and aromatic functional groups [36, 37]. The absorption band at 1,310 cm^{-1} coincides to C–C bond. Peak observed at 1,045 cm^{-1} may indicate vinyl of allicin (the principle component in garlic extract) and C–O bonds [38]. Bonds at 802 and 702 cm^{-1} could be assigned to C–O asymmetric stretching and ZnS bending bonds [39], respectively. As a result of the complex structure of capping agents sourced from the target plant, the peaks tend to broaden and combine with shoulders for different functional groups.

3.2. XRD Analysis. To inspect the purity and crystal nature of the biogenic ZnS particles, XRD analysis was performed, and the data obtained were depicted in Figure 3, compared with the standard spectra (JCPDS card no: 05-0566), and tabulated for the corresponding structural and geometry parameters in Tables 1 and 2. The results indicate cubic crystalline structure and, according to Scherrer's formula [34, 40] computed in MDI Jade6 software, the average crystallite size (D_{ave}) was 2.33 nm. Additionally, the lattice parameters a, b, and c (5.357 Å), the unit cell volume (153.732 Å^3), space group ($F43m$), and density (3.9 g/cm^3) of synthesized sample were calculated following formula described elsewhere [40, 41]. These results are comparable to some other synthesized ZnS NPs [2, 9, 42, 43]. For example, the D value calculated by XRD method for ZnS NPs obtained by, e.g., sol–gel (29.0 nm) [9], Praepagen HY (an alkyl ammonium salt; 4.8 nm) [42], solid-state (4.6), glucose-mediated (5.3) [24], starch-capped (3.3 nm) [43], polyvinyl alcohol-capped (2.9 nm) [43], and uncapped (3.7 nm) [2] were close to obtained one of 2.3 nm.

3.3. SEM Analysis. The field-emission SEM measurement was carried out to get insight into the surface morphology of ZnS NPs. The obtained FESEM micrograph is shown in Figure 4, which demonstrates particles agglomerated in a nanoscale while particles were formed in a uniform manner of shape and size, i.e., cubes and spherical shapes and calculated averaged particle sizes of 30.7 ± 5.3 nm ($n = 35$).

3.4. UV–Visible Analysis. Zinc sulfide NPs have attracted great attention because of their distinct optical properties with broad applications in optoelectronic devices and biomedical science [44, 45]. As seen in Figure 5(a), the recorded UV–vis spectra revealed an absorption decrease as wavelength increases, showing an absorption edge at about 331 nm; however, the absorption value is exclusively dependent on various factors, including the structure of the material, the size of the NPs and the defects in grain structure. Figure 5(b) also depicts the bandgap energy as determined by Tauc's plot (Equation (2)) to be 3.75 eV [46, 47].

$$\alpha h\nu = C\left(h\nu - E_g\right)^n. \tag{2}$$

In addition, the particle size for the synthesized ZnS NPs can be calculated using Brus's equation (Equation (3)) [48, 49].

$$E_{NP} - E_g = \left(\frac{h^2}{8r^2}\right)\left(\frac{1}{m_e^*} + \frac{1}{m_h^*}\right) - \left(\frac{1.8e^2}{4\pi\epsilon r^2}\right), \tag{3}$$

where E_{NP} and E_g are the bandgap of nano and bulk (3.68 eV) semiconductors, respectively, e is the electronic charge, ϵ is the dielectric constant of materials (for ZnS, $\epsilon = 8.3$), h is the Planck's constant and r is the radius of the NPs in Nanometer, m_e^* is the effective mass of the electron, m_e mass of an electron (for ZnS, $m_e^* = 0.25\ m_e$), m_h^* is the effective mass of the hole, and m_h mass of hole (for ZnS, $m_h^* = 0.60\ m_e$). Accordingly, the calculated particle size was found as 4.4 nm and being in consistence with other calculations, including XRD method.

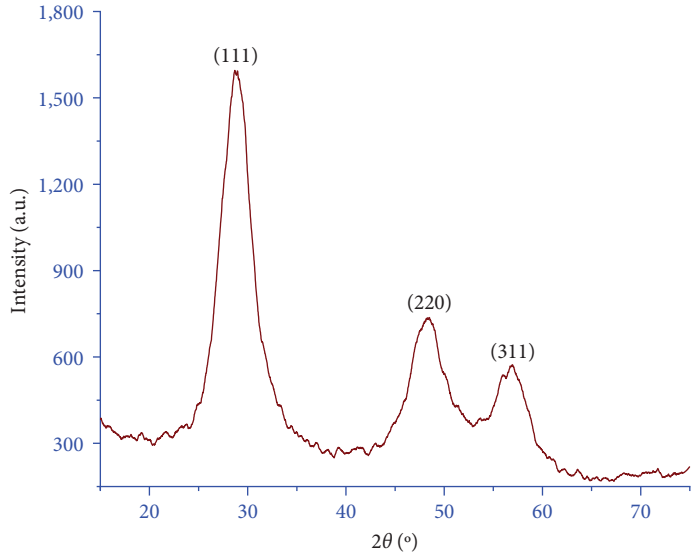

Figure 3: XRD diffractogram of ZnS NPs.

Table 1: Crystallite size (nm), FWHM, and dislocation density for ZnS NPs.

Sample	2θ (°)	(hkl)	FWHM	D (Å)	Crystallite size (nm)	Average crystallite size (nm)	Average dislocation density (lines/m^2) × 10^{17}
ZnS NPs	28.84261	(111)	3.9401	3.093	2.08204	2.32539	1.8493
	48.35156	(220)	4.0898	1.881	2.12926		
	56.59798	(311)	3.2633	1.625	2.76486		

Table 2: Geometric parameters of ZnS NPs computed based on the XRD highest intensity peak (111).

Sample	Lattice parameter; $a = b = c$ (Å)	(c/a) ratio	Volume of unit cell (Å^3)	Density (g/cm^3)	Space group
ZnS NPs	5.357	1	153.732	3.9	$F43m$

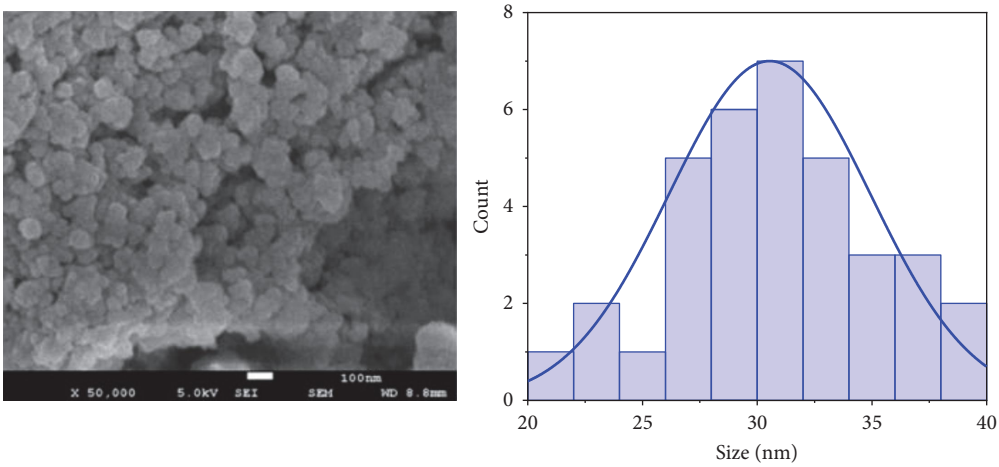

Figure 4: Field-emission scanning electron microscope (FESEM) image and particle size distribution ($n = 35$) histogram of ZnS NPs.

3.5. Antibacterial Activity. Figure 6 displays selected plate images for the antibacterial activity of the *garlic* extract-mediated synthesized ZnS NPs, 63 and 126 mg/mL, as assessed against *S. aureus* and *E. coli* bacteria species using disk diffusion method. The calculated average ZOI (diameters, mm) from two-independent experiments were collected in Table 3. It is observed that the NPs obtained in this way have comparable antibacterial activity to that of standard

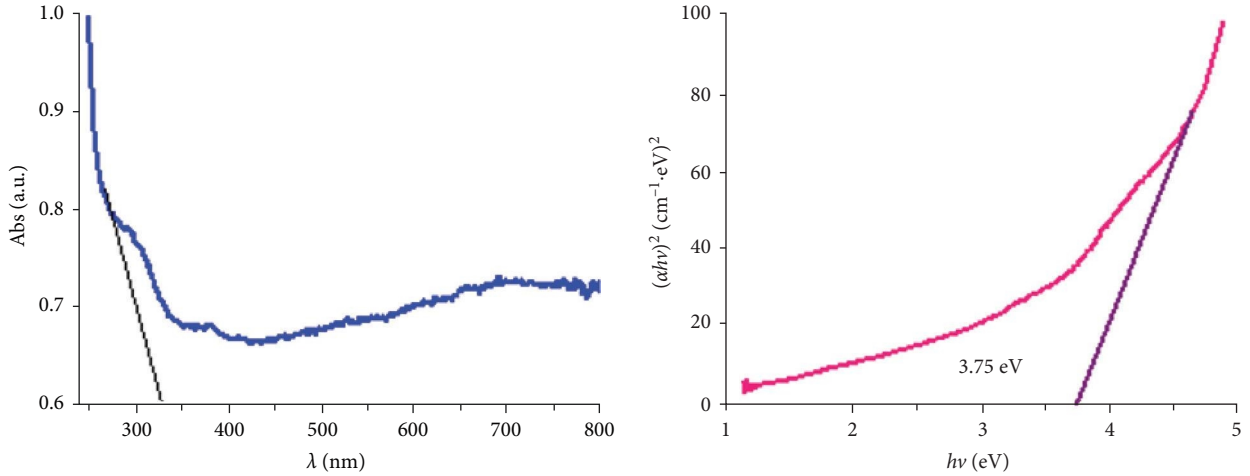

Figure 5: (a) UV–vis spectra of ZnS NPs; (b) Tauc's plot showing the optical bandgap of ZnS NPs.

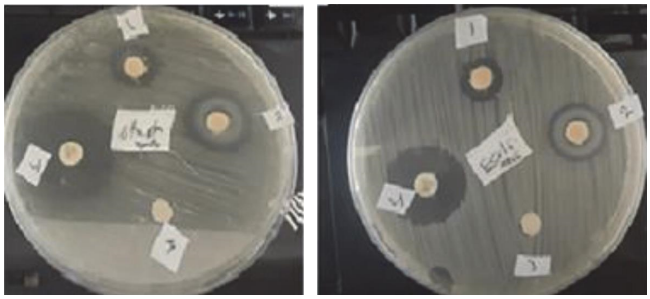

Figure 6: Selected plate images for the antibacterial activity of ZnS NPs against *S. aureus* and *E. coli* bacteria. Discs number: (1) ZnS NPs 63 mg/mL per disc, (2) ZnS NPs 126 mg/mL per disc, (3) dH_2O (negative control), and (4) azithromycin antibiotics (AzM, positive control).

Table 3: Antibacterial activity of biosynthesized ZnS NPs.

Bacteria	Zone of inhibition (ZOI; diameter in mm) ± standard deviation		
	ZnS, 63 mg/mL	ZnS, 126 mg/mL	Azithromycin standard drug
S. aureus	17 ± 1.00	23 ± 1.25	28 ± 0.50
E. coli	15 ± 0.75	18 ± 1.50	23 ± 0.75

drug as assessed against the two bacteria types, more effective on *S. aureus* than *E. coli* those representing Gram-positive and Gram-negative bacteria, respectively. Furthermore, it was found that the activity of ZnS NPs has increased as its concentration increased while being, in all cases, still slightly lower than the effect of standard drug AzM. The higher activity of metal NPs against *S. aureus* compared to *E. coli* is a result of the differences in their cell wall structures. Although the peptidoglycan in Gram-negative bacteria (e.g., *E. coli*) is thinner than that in Gram-positive, the outer membrane in the former may play a role in being less susceptible for antibiotics [32, 36]. Typically, the bioactivity of certain materials is attributed to various factors like the nature of the material, their particle size, shape, surface charge, and application conditions (e.g., concentration and exposure time). Although the mechanism involved in the inhibitory activity is still under debate, it is believed that the electrostatic attraction between the bacterial cell and ZnS NPs (and released species, e.g., Zn^{2+}, S^{2-}) plays a pivotal role. Generally, the antibacterial mechanism can go through one or simultaneous mechanisms: (1) attachment of NPs into bacterial surface; (2) releasing of ions (i.e., Zn^{2+}, S^{2-}), which could penetrate into the cell; (3) formation of reactive oxygen species, with the overall action of being led to cell destruction and death.

The antibacterial activity of some other ZnS NPs reported in literatures are given in Table 4 for comparison [9, 15, 50–52]. The ZOI as well as the test method and sample concentration were tabulated as well. Although the ZOI are seemingly higher for bio-based ZnS NPs, the test conditions (concentration and operation, in particular) differ significantly making comparison difficult. However, in each case, authors usually use standard drug as a positive control, which experimentally analyzed simultaneously with test samples. Thus, such controls can facilitate the comparison of activities and explain the results.

3.6. Hemolytic Activity on Erythrocytes. The hemolytic effect of ZnS NPs on human RBCs was in vitro assessed over a NPs concentration range of 3.12–100 μg/mL and in reference to NS and dH_2O as negative and positive controls [53], respectively. Figure 7 illustrates the average hemolytic activity from two independent experiments. In principle, the assay is based on measuring the free hemoglobin, which is released as a result of lysis induced by test samples. As can be seen, the hemolysis of ZNS NPs up to 100 μg/mL is less than 2.9%, which indicate nonhemolytic material. Basically, substances with hemolysis of less than 2% are standardized as nonhemolytic, 2%–5% slightly hemolytic, while more than 5%

Table 4: Zone of inhibition (ZOI) for antibacterial activity of ZnS NPs obtained by different synthetic methods.

Zinc sulfide; method for synthesis	Antibacterial test				Ref.
	ZOI (mm)		Method used	Conc. tested	
	S. auras	*E. coli*			
ZnS; sol–gel dip coating	7	9	Disc diffusion	6 μg/mL	[11]
ZnS; sonochemical	10	9	Disc diffusion	50 μL/disc	[17]
ZnS; sol–gel precipitation	19	22	Disc diffusion	40 mg/μL	[51]
ZnS; chemical coprecipitation	25	–	Disc diffusion	200 μL/disc	[52]
ZnS; biosynthesis	26	–	Well diffusion	200 μL/disc	[53]
ZnS; biosynthesis	23	18	Disc diffusion	126 mg/mL	This work

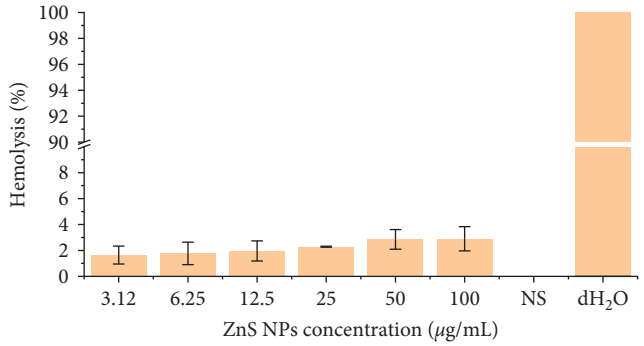

Figure 7: Hemolytic activity (%) of ZnS NPs on erythrocytes at different concentrations (3.12–100 mg/mL), NS (negative control) and dH_2O (negative control). Error bar represent standard deviation ($n = 2$).

hemolytic [53]. Herein, the lysis was considerably low, increased in a dose-dependent manner up to 2.9% at 100 μg/mL, being less than 2% up to 12.5 μg/mL and, therefore, indicating nontoxic ZnS NPs at the applied concentrations and analysis condition. Furthermore, the obtained results were close or slightly higher than that reported by other researchers for ZnS over alike concentrations [20]; however, authors investigated longer exposure time and thus detected increased hemolytic activity with extended incubation time. The hemocompatibility of erythrocytes toward ZnS NPs may ascribe a repulsive action of ZnS NPs by the cells as a result of their negative surface charge [20]. Nevertheless, such results provide preliminary data for further in deep investigation of its prospective biomedical application.

4. Conclusion

In this study, ZnS NPs were successfully synthesized first ever using garlic aqueous extract as a simple and green method. Analysis revealed a 2.33 nm crystallite cubic phase structure, 3.75 eV optical bandgap, and 30.7 nm nanoparticles by FESEM. The antibacterial test indicated comparable and dose-dependent activities, slightly below that for AzM standard drug and higher against *S. aureus* than *E. coli*. Hemolysis result, in reference to normal saline and deionized water as minimal and maximal controls, respectively, has shown negligible lysis up to 12.5 μg/mL that becomes as higher as 2.9% at 100 μg/mL. Therefore, it is concluded that the utilized bio-based method is an effective in production of ZnS NPs with desirable properties for prospective application in biomedical fields.

Data Availability

The data used to support the findings of this study are included within the article.

Conflicts of Interest

The authors declare that they have no conflicts of interest.

Acknowledgment

The authors extend their appreciation to the Deputyship for Research & Innovation, Ministry of Education in Saudi Arabia for funding this research work through the project no. (IFKSURG-2-1615). The authors are thankful to Dr. Abdullah Al-Jarfi and Dr. Morad G. S. Saleh Laps for the help with biological experiments.

References

[1] V. Chandrakala, V. Aruna, and G. Angajala, "Review on metal nanoparticles as nanocarriers: current challenges and perspectives in drug delivery systems," *Emergent Materials*, vol. 5, pp. 1593–1615, 2022.

[2] A. Alnehia, A.-B. Al-Odayni, A. Al-Sharabi, A. Al-Hammadi, and W. S. Saeed, "*Pomegranate peel* extract-mediated green synthesis of ZnO-NPs: extract concentration-dependent structure optical, and antibacterial activity," *Journal of Chemistry*, vol. 2022, Article ID 9647793, 11 pages, 2022.

[3] S. Slathia, T. Gupta, and R. P. Chauhan, "Green synthesis of Ag–ZnO nanocomposite using *Azadirachta indica* leaf extract exhibiting excellent optical and electrical properties," *Physica B: Condensed Matter*, vol. 621, Article ID 413287, 2021.

[4] M. Sharma, H. Bassi, P. Chauhan et al., "Inhibition of the bacterial growth as a consequence of synergism of Ag and ZnO: *Calendula officinalis* mediated green approach for nanoparticles and impact of altitude," *Inorganic Chemistry Communications*, vol. 136, Article ID 109131, 2022.

[5] A. Al-Sharabi, K. S. S. Sada'a, A. Al-Osta, and R. Abd-Shukor, "Structure, optical properties and antimicrobial activities of $MgO–Bi_{2-x}Cr_xO_3$ nanocomposites prepared via solvent-deicient method," *Scientiic Reports*, vol. 12, Article ID 10647, 2022.

[6] J. Koaib, N. Bouguila, H. Abassi et al., "Dielectric and electrical properties of annealed ZnS thin films. The appearance of the OLPT conduction mechanism in chalcogenides," *RSC Advances*, vol. 10, no. 16, pp. 9549–9562, 2020.

[7] U. S. Senapati and R. Athparia, "Green synthesis of ZnS nanoparticles using Allium sativum L. extract and study of their structural, optical and electrical properties," *Chalcogenide Letters*, vol. 19, pp. 203–216, 2022.

[8] A. Al-Osta, A. Alnehi, A. A. Qaid, H. T. Al-Ahsab, and A. Al-Sharabi, "Structural, morphological and optical properties of Cr doped ZnS nanoparticles prepared without any capping agent," *Optik*, vol. 214, Article ID 164831, 2020.

[9] M. Sathishkumar, M. Saroja, and M. Venkatachalam, "Influence of (Cu, Al) doping concentration on the structural, optical and antimicrobial activity of ZnS thin films prepared by sol–gel dip coating techniques," *Optik*, vol. 182, pp. 774–785, 2019.

[10] M. Wu, Z. Wei, W. Zhao, X. Wang, and J. Jiang, "Optical and magnetic properties of Ni doped ZnS diluted magnetic semiconductors synthesized by hydrothermal method," *Journal of Nanomaterials*, vol. 2017, Article ID 1603450, 9 pages, 2017.

[11] K. Benyahia, A. Benhaya, and M. S. Aida, "ZnS thin films deposition by thermal evaporation for photovoltaic applications," *Journal of Semiconductors*, vol. 36, no. 10, Article ID 103001, 2015.

[12] M. Nematollahi, X. Yang, U. J. Gibson, and T. W. Reenaas, "Pulsed laser ablation and deposition of ZnS:Cr," *Thin Solid Films*, vol. 590, pp. 28–32, 2015.

[13] A. Mukherjee and P. Mitra, "Characterization of Sn doped ZnS thin films synthesized by CBD," *Materials Research*, vol. 20, no. 2, pp. 430–435, 2017.

[14] P. Kaur, S. Kumar, A. Singh, and S. M. Rao, "Improved magnetism in Cr doped ZnS nanoparticles with nitrogen co-doping synthesized using chemical co-precipitation technique," *Journal of Materials Science: Materials in Electronics*, vol. 26, pp. 9158–9163, 2015.

[15] N. F. de Andrade Neto, P. M. de Oliveira, M. A. Corrêa, M. R. Bomio Delmonte, and F. V. da Motta, "Antimicrobial and electrical properties of ce-and ni-doped zns nanoparticles obtained by a sonochemical method," *International Journal of Applied Ceramic Technology*, vol. 18, no. 3, pp. 598–604, 2021.

[16] R. Augustine and A. Hasan, "Multimodal applications of phytonanoparticles," in *Phytonanotechnology*, pp. 195–219, Elsevier, 2020.

[17] S. H. Ansari, F. Islam, and M. Sameem, "Influence of nanotechnology on herbal drugs: a review," *Journal of Advanced Pharmaceutical Technology & Research*, vol. 3, no. 3, pp. 142–146, 2012.

[18] M. Alavi, M. R. Hamblin, and J. F. Kennedy, "Antimicrobial applications of lichens: secondary metabolites and green synthesis of silver nanoparticles: a review," *Nano Micro Biosystems*, vol. 1, no. 1, pp. 15–21, 2022.

[19] M. Alavi, M. Rai, and I. R. A. de Menezes, "Therapeutic applications of lactic acid bacteria based on the nano and micro biosystems," *Nano Micro Biosystems*, vol. 1, no. 1, pp. 8–14, 2022.

[20] J. M. Baruah, S. Kalita, and J. Narayan, "Green chemistry synthesis of biocompatible ZnS quantum dots (QDs): their application as potential thin films and antibacterial agent," *International Nano Letters*, vol. 9, pp. 149–159, 2019.

[21] A. Al-Sharabi, A. Alnehia, A. H. Al-Hammadi, K. A. Alhumaidha, and A. AL-Osta, "The effect of *Nigella sativa* seed extract concentration on crystal structure, band gap and antibacterial activity of ZnS-NPs prepared by green route," *Journal of Materials Science: Materials in Electronics*, vol. 33, pp. 20812–20822, 2022.

[22] K. Saravanadevi, M. Kavitha, P. Karpagavinayagam, K. Saminathan, and C. Vedhi, "Biosynthesis of ZnO and Ag doped ZnO nanoparticles from *Vitis vinifera* leaf for antibacterial, photocatalytic application," *Materials Today: Proceedings*, vol. 48, Part 2, pp. 352–356, 2022.

[23] M. Alavi, S. Thomas, and M. Sreedharan, "Modification of silica nanoparticles for antibacterial activities: mechanism of action," *Micro Nano Bio Aspects*, vol. 1, no. 1, pp. 49–58, 2022.

[24] U. S. Senapati, D. K. Jha, and D. Sarkar, "Green synthesis and characterization of ZnS nanoparticles," *Research Journal of Physical Sciences*, vol. 1, no. 7, pp. 1–6, 2013.

[25] S. Z. Rahchamani, H. R. Dizaji, and M. H. Ehsani, "Study of structural and optical properties of ZnS zigzag nanostructured thin films," *Applied Surface Science*, vol. 356, pp. 1096–1104, 2015.

[26] S. G. Santhosha, P. Jamuna, and S. N. Prabhavathi, "Bioactive components of garlic and their physiological role in health maintenance: a review," *Food Bioscience*, vol. 3, pp. 59–74, 2013.

[27] G. El-Saber Batiha, A. M. Beshbishy, L. G. Wasef et al., "Chemical constituents and pharmacological activities of garlic (*Allium sativum* L.): a review," *Nutrients*, vol. 12, no. 3, Article ID 872, 2020.

[28] H. A. R. Suleria, M. S. Butt, F. M. Anjum, F. Saeed, R. Batool, and A. N. Ahmad, "Aqueous garlic extract and its phytochemical profile; special reference to antioxidant status," *International Journal of Food Sciences and Nutrition*, vol. 63, no. 4, pp. 431–439, 2012.

[29] G. Von White, P. Kerscher, R. M. Brown et al., "Green synthesis of robust, biocompatible silver nanoparticles using garlic extract," *Journal of Nanomaterials*, vol. 2012, Article ID 730746, 12 pages, 2012.

[30] A. A. Alyamani, S. Albukhaty, S. Aloufi, F. A. AlMalki, H. Al-Karagoly, and G. M. Sulaiman, "Green fabrication of zinc oxide nanoparticles using *Phlomis* leaf extract: characterization and in vitro evaluation of cytotoxicity and antibacterial properties," *Molecules*, vol. 26, no. 20, Article ID 6140, 2021.

[31] W. Ahmad and D. Kalra, "Green synthesis, characterization and anti microbial activities of ZnO nanoparticles using *Euphorbia hirta* leaf extract," *Journal of King Saud University - Science*, vol. 32, no. 4, pp. 2358–2364, 2020.

[32] A. Rahman, M. H. Harunsani, A. L. Tan, N. Ahmad, B.-K. Min, and M. M. Khan, "Influence of Mg and Cu dual-doping on phytogenic synthesized ZnO for light induced antibacterial and radical scavenging activities," *Materials Science in Semiconductor Processing*, vol. 128, Article ID 105761, 2021.

[33] M. M. S. Saif, R. M. Alodeni, A. A. Alghamdi, and A.-B. Al-Odayni, "Synthesis, spectroscopic characterization, thermal analysis and *in vitro* bioactivity studies of the *N*-(cinnamylidene) tryptophan Schiff base," *Journal of King Saud University - Science*, vol. 34, no. 4, Article ID 101988, 2022.

[34] A. Alnehia, A. H. Al-Hammadi, A. Al-Sharabi, and H. Alnahari, "Optical, structural and morphological properties of ZnO and Fe^{+3} doped ZnO-NPs prepared by *Foeniculum vulgare* extract as capping agent for optoelectronic applications," *Inorganic Chemistry Communications*, vol. 143, Article ID 109699, 2022.

[35] M. Jothibas, C. Manoharan, S. Johnson Jeyakumar, P. Praveen, I. Kartharinal Punithavathy, and J. Prince Richard, "Synthesis and enhanced photocatalytic property of Ni doped ZnS nanoparticles," *Solar Energy*, vol. 159, pp. 434–443, 2018.

[36] N. A. Al-Shabib, F. M. Husain, F. Ahmed et al., "Biogenic synthesis of Zinc oxide nanostructures from *Nigella sativa* seed: prospective role as food packaging material inhibiting broad-spectrum quorum sensing and biofilm," *Scientific Reports*, vol. 6, Article ID 36761, 2016.

[37] C. A. Soto-Robles, P. A. Luque, C. M. Gómez-Gutiérrez et al., "Study on the effect of the concentration of *Hibiscus sabdariffa* extract on the green synthesis of ZnO nanoparticles," *Results in Physics*, vol. 15, Article ID 102807, 2019.

[38] T. P. Nguyen, Q. V. Lam, and T. B. Vu, "Energy transfer in poly(vinyl alcohol)-encapsulated Mn-doped ZnS quantum dots," *Journal of Luminescence*, vol. 203, pp. 533–539, 2018.

[39] S. C. Tudu, M. Zubko, J. Kusz, and A. Bhattacharjee, "Structural, morphological and optical characterization of green synthesized ZnS nanoparticles using Azadirachta Indica (Neem) leaf extract," *International Journal of Nano Dimension*, vol. 11, pp. 99–111, 2020.

[40] A. AL-Osta, A. Alnehia, A. A. Qaid, H. T. Al-Ahsab, and A. Al-Sharabi, "Structural, morphological and optical properties of Cr doped ZnS nanoparticles prepared without any capping agent," *Optik*, vol. 214, Article ID 164831, 2020.

[41] M. S. Nadeem, T. Munawar, F. Mukhtar et al., "Hydrothermally derived Co, Ni co-doped ZnO nanorods; structural, optical, and morphological study," *Optical Materials*, vol. 111, Article ID 110606, 2021.

[42] J. K. Salem, T. M. Hammad, S. Kuhn, M. A. Draaz, N. K. Hejazy, and R. Hempelmann, "Structural and optical properties of Co-doped ZnS nanoparticles synthesized by a capping agent," *Journal of Materials Science: Materials in Electronics*, vol. 25, pp. 2177–2182, 2014.

[43] T. Xaba, "Green synthesis of ZnS nanoparticles and fabrication of ZnS–chitosan nanocomposites for the removal of Cr(vi) ion from wastewater," *Green Processing and Synthesis*, vol. 10, no. 1, pp. 374–383, 2021.

[44] M. S. Khan, L. Shi, B. Zou, and H. Ullah, "Effect of vanadium doping on optoelectronic and magnetic properties of wurtzite ZnS crystal," *Optik*, vol. 204, Article ID 164162, 2020.

[45] M. Ashokkumar and A. Boopathyraja, "Structural and optical properties of Mg doped ZnS quantum dots and biological applications," *Superlattices and Microstructures*, vol. 113, pp. 236–243, 2018.

[46] A. Derbali, A. Attaf, H. Saidi et al., "Investigation of structural, optical and electrical properties of ZnS thin films prepared by ultrasonic spray technique for photovoltaic applications," *Optik*, vol. 154, pp. 286–293, 2018.

[47] A. Al-Sharabi, A. Alnehia, A. AL-Osta, and N. A. A. Yahya, "Effect of copper doping on structural and optical properties of zinc sulfide (ZnS) nanoparticles," *Al-Baydha University Journal for Researches*, vol. 1, no. 2, pp. 224–233, 2019.

[48] S. Sapra and D. D. Sarma, "Evolution of the electronic structure with size in II–VI semiconductor nanocrystals," *Physical Review B*, vol. 69, no. 12, Article ID 125304, 2004.

[49] S. Kumar, H. C. Jeon, T. W. Kang, R. Singh, J. K. Sharma, and R. K. Choubey, "Structural and optical properties of silica capped ZnS:Mn quantum dots," *Journal of Materials Science: Materials in Electronics*, vol. 26, pp. 3939–3946, 2015.

[50] S. Vijayan, C. S. Dash, G. Umadevi, M. Sundararajan, and R. Mariappan, "Investigation of structural, optical and antibacterial activity of ZnS nanoparticles," *Journal of Cluster Science*, vol. 32, pp. 1601–1608, 2021.

[51] M. Wadhwani and S. Jain, "Synthesis and antimicrobial activity of zinc sulphide nanoparticles," *Research Journal of Recent Sciences*, vol. 34, pp. 36–39, 2015.

[52] C. Malarkodi, S. Rajeshkumar, K. Paulkumar, M. Vanaja, G. Gnanajobitha, and G. Annadurai, "Biosynthesis and antimicrobial activity of semiconductor nanoparticles against oral pathogens," *Bioinorganic Chemistry and Applications*, vol. 2014, Article ID 347167, 10 pages, 2014.

[53] D. Guowei, K. Adriane, X. Z. Chen, C. Jie, and L. Yinfeng, "PVP magnetic nanospheres: biocompatibility, in vitro and in vivo bleomycin release," *International Journal of Pharmaceutics*, vol. 328, no. 1, pp. 78–85, 2007.